Intra-night flickering of RS Ophiuchi: IV. Shapes of repeating time structures and their evolution

Ts. B. Georgiev[1], R. K. Zamanov[1], S. Boeva[1], G. Latev[1], B. Spassov[1], J. Martí[2], G. Nikolov[1], S. Ibryamov[3], S. V. Tsvetkova[1], K. A. Stoyanov[1]

[1] Institute of Astronomy and National Astronomical Observatory, Bulgarian Academy of Sciences, 72 Tsarigradsko Chaussee Blvd., 1784 Sofia, Bulgaria

[2] Departamento de Físika (EPSJ), Universidad de Jaén, Campus Las Lagunillas A3-420, 23071 Jaén, Spain

[3] University of Shumen, 115, Universitetska Str., 9700 Shumen, Bulgaria

tsgeorg@astro.bas.bg

(Submitted on 21.07.2019. Accepted on 25.05.2020)

Abstract. The flickering of the recurrent nova RS Oph is studied by 58 light curves (LCs), taken by 5 telescopes in 2008–2017. The light curves of the flickering source are derived after removal of the contribution of the red giant and account of the interstellar extinction. Many LCs show repeating time structures with approximately similar shapes. In this work we select 25 LCs (12 in B band and 13 in V band), with monitoring times 62–223 min, where the main time structures with quasi-periods 16–56 min repeat 3–7 times. We derive combined (averaged) profiles the structure and characterize them by shape parameters. The average SNR of the combined profiles is 26, from 10 to 43. In 2009–2017 the asymmetry (skewness) of the shape varies gradually from positive to negative. Simultaneously, higher brightness and redder color indexes of the flickering source (in 2009–2010 or 2016–2017) correspond to positive or negative asymmetry of the combined profile.

Key words: stars: binaries: symbiotic – novae, cataclysmic variables – accretion, accretion discs – stars: individual: RS Oph

Introduction

RS Oph is a symbiotic recurrent nova containing an M2 III mass donor (She-navrin, Taranova & Nadzhip 2011) and a massive carbon-oxygen white dwarf (Mikolajewska & Shara 2017). The flickering of RS Oph (brightness variability on time scales from minutes to hours) has been firstly detected by Walker (1977). Wynn (2008) proposed that both Roche lobe overflow and stellar wind capture are possible accretion scenarios in the case of RS Oph. Kundra, Hric & Gális (2010) carried out wavelet analysis of flickering light curves (LCs) unveiled flickering quasi-periods (QPs) with modes at 15–30 min and > 30 min. Later, Kundra & Hric (2014) revealed QP modes at 10 min and 24 min.

Zamanov et al. (2018) derived the apparent magnitudes of the red giant, $m_{\rm B} = 14.66$ mag and $m_{\rm V} = 12.26$ mag, as well as interstellar extinction toward RS Oph, $E(B-V) = 0.69$. This ensures the study of the behavior of the flickering source (FS) in the linear scale of fluxes. Zamanov et al. (2018) found that RS Oph becomes bluer as it becomes brighter, but the FS becomes redder as it becomes brighter. No correlation between the temperature of the FS and the brightness of FS was found. However, correlation coefficient 0.81 between the B-band magnitude and the average radius of the flickering source was revealed, i.e. as the brightness of the system increases, the size of the flickering source also increases.

In Paper I (Georgiev et al. 2019), working in magnitude scales, flattened the LCs by linear regression and found repeating flickering structures in all 58 LCs. In Paper II, working in linear scales of fluxes, flattened the LCs by low degree polynomials, Georgiev et al.(2020a) and unveiled 97 QPs, detected by local minima of structure functions and local maxima of autocorrelation functions.

In Paper II the distribution of the QPs shows modes at 8, 13, 21, 30, 48 and 73 min (the mode at 8 min is badly pronounced). These modes follow a power function with base 1.55 within standard deviation 4.7%. This power function, hinting about some 3/2 resonance, predicted modes at 5.3 and 3.5 min, which are not detectable in the whole LCs. In Paper III (Georgiev et al. 2020b), using suitable parts of the LCs, unveiled 63 QPs in the minute scale and confirmed the QP modes at 8.0, 5.3 and 3.5 min. Typical intra-night evolutions of the shortest QPs is shown too.

In this Paper IV we concentrate on the shapes of the repeating time structures and their evolution during the years. The purpose is deriving of combined (averaged) profiles (CPs) of the repeating time structures and studying of their structure and evolution. The contents follows.
1. Observing material and deriving of combined profiles.
2. Signal-to-noise ratios of the combined profiles.
3. Asymmetry and excess of the shapes of the combined profiles in 2009–2017.
4. Asymmetry versus brightness or color index of the flickering source.
Conclusions; Bibliography; Appendix.

The Appendix contains 24 panels with light curves and combined profiles, similar to these in Fig. 2.

Abbreviations and subscripts:
AV – average value;
CP – combined profile;
FS – flickering source;
GR – gradient (slope coefficient) of regression line;
LC – flickering light curve;
MT – monitoring time, in minutes;
QP – flickering quasi-period, in minutes;
SD – standard deviation;
SNR – signal-to-noise ratio.

1. Observing material and deriving of combined profiles

We analyze 58 linearized LCs of the FS (28 in B band, 29 in V band), taken in 2009–2017 by 5 telescopes. The apparent magnitude of RS Oph is 10–11 mag. The standard error of the photometry is 0.005–0.010 mag. The observing material is described in the paper of Zamanov et al. (2018) and in Paper II. The details of the processing are described in Paper II. For this work we selected 25 LCs (12 in B band and 13 in V band) in which the main time structures repeat 2.8–7.1 times, changing to some extent their shapes. Data about the selected LCs are given in Table 1 and Table 2.

Table 1. Data about the observing material and processing results. 1 – designation of the (residual relative) light curve as in Paper II, Fig. 2 and Appendix B; 2 – year of the monitoring; 3 – time duration of the monitoring, [min]; 4 – number of data in the monitoring; 5 – average time step of the monitoring, [min]; 6 – quasi-period, [min]; 7 – number of quasi-periods inside the light curve; 8 – standard deviation S of the light curve, [%]; 9 – standard deviation $g_{\rm AV}$ of the combined profile, [%]; 10 – height H of the combined profile, [%]; 11 – signal-to-noise ratio SNR, Sect. 2; 12 – SNR, [dB], Sect. 2; 13 – Asymmetry (skewness, Sect. 3); 14 – Excess (kurtosis, Sect. 3) .

#	Year	$T_{\rm M}$	n	$\tau_{\rm M}$	QP	q	S	$g_{\rm AV}$	H	SNR	$SNR_{\rm dB}$	A	E
1	2	3	4	5	6	7	8	9	10	11	12	13	14
03b	2009.46	103.7	83	1.26	29.5	3.52	5.26	3.43	7.00	26.7	14.3	0.275	–0.869
07b	2010.33	109.9	66	1.69	28.0	3.93	4.75	3.86	4.85	21.5	13.3	0.589	–1.004
10B	2012.55	126.6	314	0.40	21.0	6.03	4.43	3.63	4.49	18.6	12.7	–0.069	–0.865
11B	2012.56	220.7	200	1.11	56.0	3.94	5.59	4.28	5.92	30.3	14.8	0.555	–0.293
12B	2012.63	148.0	83	1.80	51.0	2.90	4.51	3.16	5.80	19.3	12.9	1.179	0.427
13B	2012.63	127.2	223	0.57	20.0	6.36	4.58	3.84	4.76	20.0	13.0	–0.136	–0.651
14B	2013.51	121.4	46	2.70	31.0	3.92	5.78	3.49	7.73	32.4	15.1	–0.450	–0.668
16B	2013.62	160.6	470	0.34	47.0	3.42	5.01	3.11	5.76	24.2	13.8	–0.386	–1.019
20B	2014.48	121.2	106	1.15	17.0	7.13	4.89	4.03	5.32	22.9	13.6	–0.473	–0.026
27B	2017.49	124.8	148	0.85	30.0	4.16	4.13	2.99	5.05	16.1	12.1	–0.800	–0.210
28B	2017.55	119.2	129	0.93	23.0	5.18	3.98	3.09	4.27	14.8	11.7	–0.220	–1.033
29B	2017.68	63.0	66	0.97	16.0	3.94	3.88	3.09	4.34	14.0	11.5	–0.071	–0.684
03v	2009.46	102.3	133	0.78	29.0	3.53	5.55	4.54	5.31	29.8	14.7	0.303	–0.796
07V	2010.33	115.6	67	1.75	28.0	4.13	5.66	4.87	5.51	31.1	14.9	0.438	–0.930
08V	2012.32	96.3	141	0.68	21.0	4.59	6.63	5.33	6.89	43.0	16.3	–0.524	0.349
10V	2012.55	115.9	200	0.58	21.0	5.52	5.56	4.28	6.25	29.9	14.8	–0.156	–0.813
11V	2012.56	223.5	220	1.02	56.0	3.99	6.66	5.63	6.11	43.3	16.4	0.301	–0.716
12v	2012.63	134.3	70	1.95	47.0	2.86	6.35	4.18	7.58	39.3	15.9	0.815	–0.074
13V	2012.63	124.0	224	0.56	20.0	6.20	6.02	3.92	8.20	35.3	15.5	0.047	–0.884
14V	2013.51	121.4	47	2.64	31.5	3.86	6.47	5.27	7.61	40.9	16.1	–0.302	–0.681
16V	2013.62	137.6	335	0.41	47.0	2.93	6.46	4.18	8.10	40.7	16.1	-0.407	–0.811
17V	2013.62	142.5	361	0.40	28.0	5.09	5.97	4.83	5.96	34.7	15.4	–0.061	-0.999
27V	2017.49	120.4	145	0.84	29.0	4.15	3.92	2.98	4.47	14.4	11.6	–0.612	–0.003
28V	2017.55	119.2	129	0.93	23.0	5.18	3.97	3.05	4.27	14.8	11.7	–0.291	–0.911
29V	2017.90	62.1	67	0.94	16.0	3.88	3.34	2.62	3.61	10.2	10.1	–0.011	–0.870

Table 2. Statistics of the observations and results. (The individual data are collected in Table 1.) $T_{\rm M}$ [min] – time duration of the monitoring; n – number of data points in the monitoring; $\tau_{\rm M}$ [min] – average time step of the monitoring; QP [min] – quasi-period of the repeating structure; q – number of quasi-periods in the LC; S [%] – SD of the LC, Fig. 1 and 2; $S_{\rm SD}$ [%] – calculated SD of S, Sect. 1, not included in Table A1; $g_{\rm AV}$ – average SD of the points G_k of the CP, H [%] – height of the CP, Fig. 1 and 2, Eqs. 4; SNR – signal-to-noise ratio (Eqs. 5); $SNR_{\rm dB}$ – signal-to-noise ratio in dB (Eqs. 5); A – asymmetry (skewness) of the CP (Fig. 6(a)); E – excess (kurtosis) of the CP (Fig. 6(b)).

Parameter	AV	SD	Min	Max	Text
$T_{\rm M}$	126	36	62	223	Sect. 1
n	163	110	46	470	Sect. 1
$\tau_{\rm M}$	1.09	0.66	0.34	2.70	Sect. 1
QP	30	12	16	56	Sect. 1
q	4.4	1.1	2.8	7.1	Sect. 1
S	5.17	0.99	3.34	8.66	Sect. 1
$S_{\rm SD}$	0.34	0.13	0.16	0.68	Sect. 1
$g_{\rm AV}$	3.9	0.8	2.6	5.6	Sect. 1
H	5.81	1.33	3.61	8.20	Sect. 1
SNR	26.7	10.2	10.2	43.3	Sect. 2
$SNR_{\rm dB}$	13.9	1.8	10.1	16.4	Sect. 2
A	–0.02	0.48	–0.88	1.18	Sect. 3
E	–0.60	0.44	–1.03	0.44	Sect. 3

As in Paper II, we explore residual relative LCs $\delta b(t)$ or $\delta v(t)$. They are derived from the preliminary linearized (in fluxes) LCs $b(t)$ or $v(t)$,

$$\delta b(t) = [b(t) - b_p(t)]/b_p(t) \quad \text{or} \quad \delta v(t) = [v(t) - v_p(t)]/v_p(t). \tag{1}$$

Here $b_p(t)$ or $v_p(t)$ is a low degree polynomial which fits the large scale trend of the linearized LC.

Let us to denote the (residual relative) LCs from Eqs. 1 by $F_i(t_i)$. By deriving the average value (AV) of such LC is 0. Let us also to denote the standard deviation of such LC by S. Then the main properties of the LCs $F_i(t_i)$, used here, are:

$$F_{\rm AV} = 0 \quad \text{and} \quad F_{\rm SD} = S. \tag{2}$$

We express the LCs, their SDs and other parameters in percents.

Figure 1 illustrates the derivation of a CP $G_k(t_k)$, shown in Fig. 2(b), from the LC $F_i(t_i)$, shown in Fig. 2(a). The monitoring time is 96 min, the number of points is 141, the time resolution is 0.7 min and the SD is 6.6%. The main (dominating) QP of 21 min is 4.6 times shorter than the monitoring time.

In Fig. 1(a) 4.6 consecutive parts of the LC are put with common zero-point in a 21 min time interval. The duration of the last added part is 0.6×21 min. Later on, these are ordered by time. Figure 1(b) shows the relevant CP $G_k(t_k)$, build for $m = 20$ points, with individual SDs g_k and AV of these SDs $g_{Av} = 5.2\%$. The number of points m for different CPs is 12–30, chosen to ensure at least 5 LC points for each CP point. The vertical tic mark $t_0 = 1$ min is the position of the minimum of this CP,

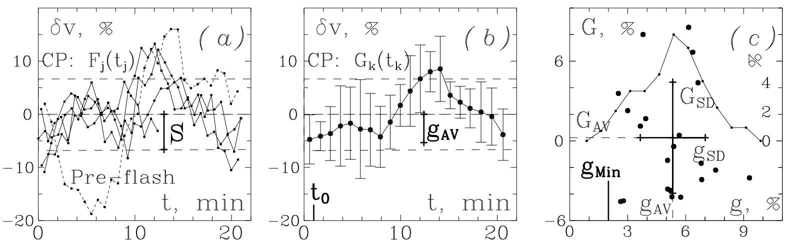

Fig. 1. (**a**): Preliminary CP $Ff_j(t_j)$ which is an overlay of 4.6 consecutive parts of the LC, shown in Fig. 2(a). The vertical segment S visualizes the SD and the horizontal lines show $\pm SD$ of the LC. Short-dashed broken line shows a strong pre-flash plus flash with common duration about 15 min. (**b**): The points of the CP G_k, their individual SDs g_k and the average of these SDs $g_{\rm AV}$. The point $t_0 = 1$ min corresponds to the minimum of this CP, chosen to be the zero-point phase in Fig. 2. (**c**): Juxtaposition of the CP points G_k and their SDs g_k. The error bars visualize the SDs $G_{\rm SD}$ and $g_{\rm SD}$. The curve (with tic marks on the right ordinate axis) shows the histogram of the SDs g_k. The value $g_{\rm Min}$ is the left bound of the SDs of the CP points.

derived additionally to be the phase zero-point in resulting CPO (Fig. 2). Figure 1*c* juxtaposes the CP points G_k and their SDs g_k and shows the histogram of the SDs g_k.

Figure 1 illustrates common particularities of all CPs. The parts of the LC in the overlay (Fig. 1(a)) have roughly similar shapes and by this reason the SDs of the CP points (Fig. 1(b)) are large and the histogram of the SDs g_k of the CP points (Fig. 1(c)) is wide. The minimal SD $g_{\rm Min}$, as in the majority LCs (Paper II), seems to be 2%.

Note that in this and some other LCs (see the Appendix), an extraordinary event (pre-flash plus flash) increases significantly the SDs of some CP points and changes the shape of the CP. It causes local minimum and increases the global maximum of the CP. Generally, the SDs g_k are large and the signal-ro-noise ratio (SNR) of these CPs ought to be low (Sect. 2).

Figure 2(a) shows the LC (#08V). The vertical segments bound 4.6 repetitions of its QP of 21 min. The places of the vertical segments correspond to minima in the LC, connected with the zero phase of the periodicity. Figure 2(b) shows 2 periods of the CP $G_k(t_k)$, shifted by time t_0=1 min for coinciding between the zero-phase and minimum of the CP.

The CP of a repeating time structure may be characterized by its peak-to-peak amplitude and average SD of its points. However, the values $G_{\rm Max}$ and $G_{\rm Min}$ have large SDs g. For this reason we include in the considerations the average height of the CP, H, with SD $H_{\rm SD} = g_{\rm AV}$. Both based on all m CP points :

$$H = 2 \times < |G_k| > \quad \text{and} \quad H_{\rm SD} = \; < g_k >, \quad k = 1, ..., m. \qquad (3)$$

Here "$< . >$" means average value and "$2\ \times$" is need for H to compensate the fact that te zero point of the values of F and G lies among the LC data.

Other 24 LCs and CPs are included in the Appendix. All CPs of LCs are smoothed slightly by convolution kernel [0.25, 0.5, 0.25]. The parameters of the LCs and their CPs are collected in Table 1.

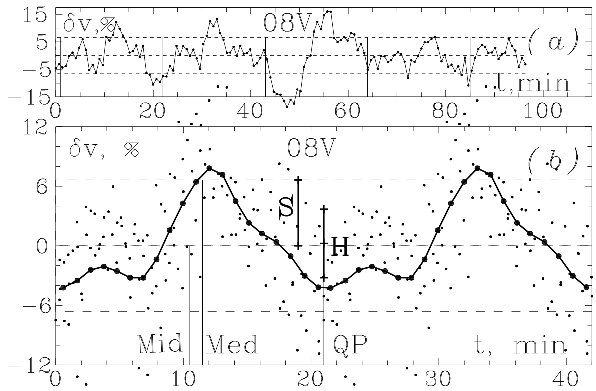

Fig. 2. (**a**): The residual LC #08V (analyzed in Paper II) with repeating time structures, bound by vertical segments. (**b**): Two CPs for this LC. Vertical segments visualize the SD S of the LC and the height H of the CP. Horizontal dashed lines bound the ± SD interval of the LC. "Mid" and "Med" are the middle and the median time points of the CP.

In this work we unveil repeating time structures among the apparent chaos of the flickering LC. Therefore, an application of our approach on known time series is necessary, as in Paper II.

Figure 3, top panels, shows the variations of the Wolf index, $W(t)$, containing faint short-time fluctuations and well pronounced large-time cycle, as well as the relevant CP. The variations of the planetarium visits, $N(t)$, containing strong short-time fluctuations and poorly pronounced large-time cycle, as well as the relevant CP, are shown in Fig. 3, bottom panels. The monitoring times are 1950–2018 and 2013–2018. Time resolutions are 2 months and 1 week. The durations of the cycles are 10.7 years and 1 year. The numbers of the covered cycles are 6.3 and 6.0, respectively.

For these time series $W(t)$ and $N(t)$ the values of H are 115 and 82%, of S are 74 and 62%, as well of $g_{\rm AV}$ are 36 and 34%, respectively. The CP of N shows 6 sub-cycles per year with duration 2 months. The reason is the specific time-table of the pupils and students.

Figure 4 presents the distribution of the CP points G_K and their SDs g_K of the time series $W(t)$ and $N(t)$, shown in Fig. 3. The purpose is estimations of the minimal SDs $g_{\rm min}$, which are necessary for the SNRs in Sect. 2. Here the minimal SDs are adopted to be 5% and 10%, respectively.

2. Signal-to-noise ratios of the combined profiles

The "goodness" of the CP may be characterized by its signal-to-noise ratio (SNR). In our cases the values of the CP points and their individual SDs are mutually compatible (Fig. 1(b,c)) and we have to expect low SNRs.

We consider that the signal is random variable with $AV = H$ and $SD = S$, which is added to random noise with expected mean of zero and finite $SD = s$. Two "intuitive" ratios are used in experimental and

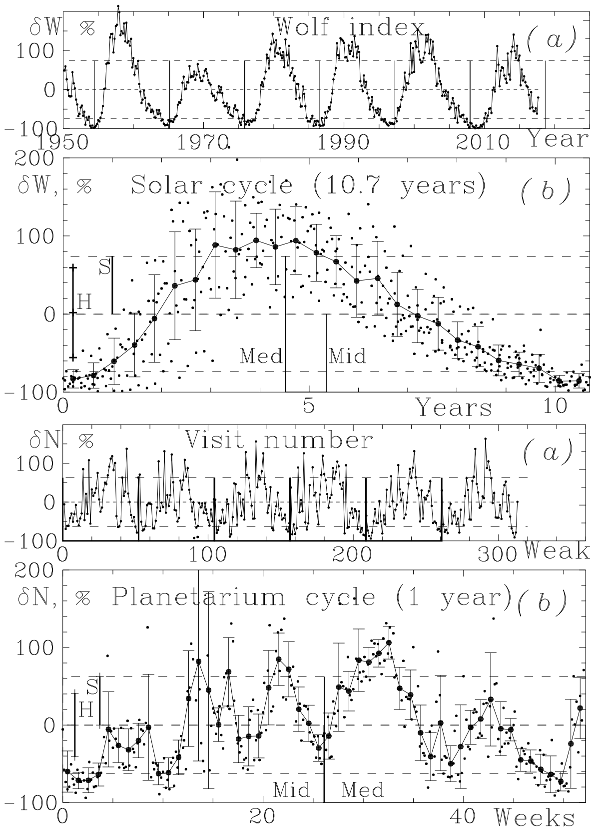

Fig. 3. Residual relative time series and their CPs of the Wolf index W (top pair panels) and planetarium visits N (bottom pair panels). Only one period is shown without smoothing. The SD S (Eqs. 2) of the LC, as well as the average height H (Eq. 3) of the CP are shown in the left parts of the diagrams. See Fig. 2 for details.

engineering practice to characterize the superiority of the signal over the noise:

$$\mathrm{SN}_1 = H/s \quad \text{and} \quad \mathrm{SN}_2 = S/s. \tag{4}$$

The conventional SNR is defined as ratio between the powers of the signal and noise (Johnson 2006). In practice the ratio between the dispersions of the signal and noise is used. Then the SNR and SNR, expressed in decibels are:

$$SNR = (S^2 - s^2)/s^2 = SN_2^2 - 1 \quad \text{and} \quad SNR[\mathrm{dB}] = 10 \times \lg\ (SNR). \tag{5}$$

So, 4 ratios, based on H, S and s may characterize the goodness of every CP (Eqs. 4 and 5). We concentrate on SN_1 and SNR.

We have well derived height H of the CP (Eqs. 3). However, the average SD of H, $h = \; < g_k >$ (Eqs. 3) is relatively large, about 2 times lower than

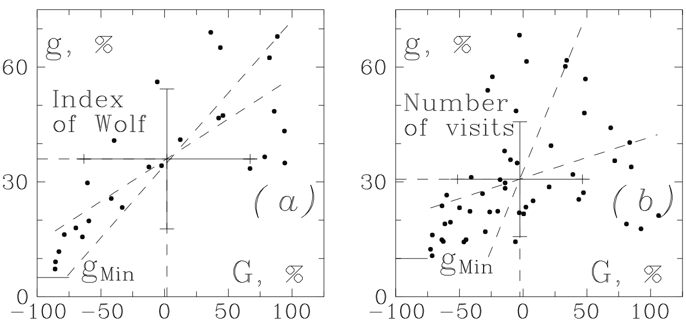

Fig. 4. Juxtaposition of the CP points G_k and their SDs g_k from the CPs of the time series $W(t)$ and $N(t)$, in Fig. 3. Dashed lines show the ordinary and reverse regressions. Error crosses show the SDs of the compared values. Horizontal tic marks show the estimations of the minimal SDs of the CP points.

S. (Table 1, Table A1). Therefore, our SN_1 ratio is poorly estimated. We have also well derived SD S for every LC. It has relatively low formal SD $s_{\rm SD} = S/[2(n-1)]^{1/2}$, 10–15 times lower than S. Therefore our SN_2 ratio seems to be better derived.

While H and S are derivable, the SD of the noise, s, may be estimated only indirectly. The simplest solution is adoption that s is the photometric standard error. In Fig. 1(c) and in the majority of the CPs in the Appendix B, the minimal standard deviation of the profile points, $s = g_{\rm Min}$ seems to be $s \approx 2\%$. However, simple parts of the LCs, analyzed in Paper III for detection of short quasi-periods, give evidences that $s \approx 1\%$. On the other hand, our observing practice shows the same, $s \approx 0.01$ mag, i.e. again $\approx 1\%$. Therefore, we may consider that the SD of the noise in our LCs and CPs is

$$s = 1\%. \tag{6}$$

However, the SD of s rest unknown, the SD of any SNR estimation too.

Adopting $s = 1\%$ leads to ultimate simplifications:

$${\rm SN}_1 = H \qquad \text{and} \qquad {\rm SN}_2 = S, \tag{7}$$

Thus, the values of H and S, expressed in percents, are parameters of the CPs. Simultaneously, they are dimensionless measures of the simplest forms of the SNR estimation, H/s and S/s (Eqs. 4).

Concrete numerical results follow. For the LC #08V (Fig. 2), with $s =$ 1%, we have $SN_1 = 6.9$, $SN_2 = 6.6$, $SNR = 43 = 16.3$ dB. For the index of Wolf, with $s = 5\%$ (Fig.4(a)), we have 14.8, 23, 530 and 27.2 dB, respectively. For the planetarium visits, with $s = 10\%$ (Fig.4(b)), we have 8.2, 7.3, 38 and 15 dB, respectively. But in two cases the used values of s seem to be overestimated and, therefore, out SNR values ought to be underestimated. Statistics of the SNR parameters for the CPs are collected in Table 1. From this point of view the flickering of RS Oph again is similar to the variations of the planetarium visits.

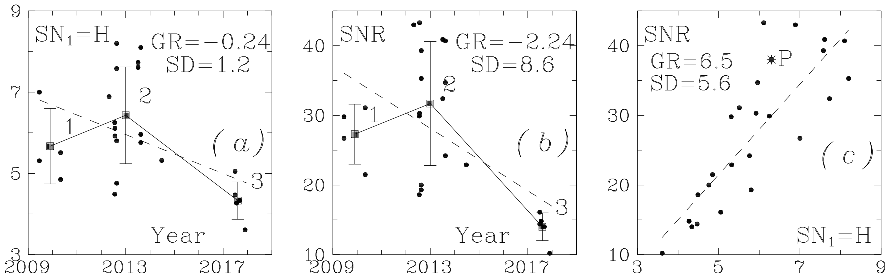

Fig. 5. (**a,b**): Course of SN_1 (Eqs. 6) and SNR (Eqs. 5) in 2009–2017; The error bars correspond to time periods 1, 2 and 3 (see the text); (**c**): Juxtaposition of SN_1 and SNR. Dashed lines represent regressions. The relevant gradients, GR, and standard deviation, SD, are implemented; In (**c**) the position of the CP of the number of the planetarium visits is shown by P and a square. The position of the CP of the index of Wolf lies far out of this diagram.

Figure 5 shows the behavior of SN_1 and SNR through the years and compares them in a common diagram. Here the used 25 CPs are divided by years into 3 groups: Group 1 – 2009–2010, 4 COs, Group 2 – 2012–2015, 15 COs and Group 3 – 2017–2018, 6 CPs.

Generally, the CPs are characterized by low SNRs with approximately derived values. In spite of this, in the years the SNR obeys some decreasing. Figures 5(a) and 5(b) give evidence also about some decrease of the SNR of the CPs through the years. Figure 5(c) shows that the values of the conventional SNR are about 6.5 times larger than the simple ratio SN_1.

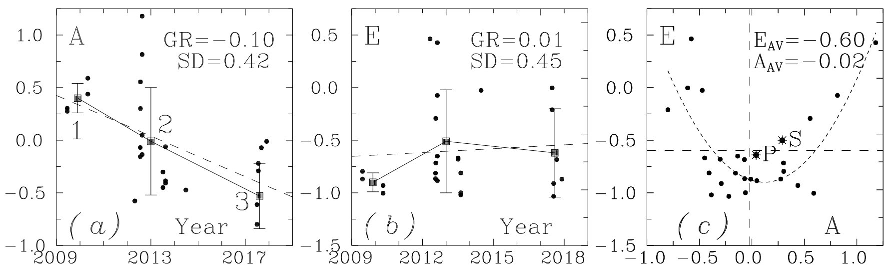

Fig. 6. (**a,b**): Evolution over the years of the asymmetry A and the excess E (dots). Large dots and error bars represent the data, divided in 3 time intervals (see the text). Dashed lines represent regressions of those parameters that are implemented; (**c**) Juxtaposition of A and E. Dashed lines show the average values of A and E. Short dashed curve corresponds to 2-nd degree polynomial.

3. Asymmetry and excess of the shapes of the combined profiles in the period 2008–2017

The shape of any finite distribution, including every our CP, may be characterized by its dimensionless parameters asymmetry (skewness) A and excess (kurtosis) E. The conventional definition and formulas are given in Paper II. The statistics of the asymmetry and excess for our 25 CPs are collected in Table 1.

Figure 6 represents asymmetry A and excess of our 25 CPs, shown in Fig. 2(b) and in each (b) sub-figure in Appendix B. Figure 6(a) shows that the asymmetry decreases gradually from positive to negative values. The CP shape is average symmetric in 2013-2014. Figure 5(b) does not show some tendency of the excess. However, according to Fig. 6(c), the asymmetry and the excess seem to be connected to some extent. Large excess corresponds to large absolute value of the asymmetry.

Statistics of the asymmetry and excess for our 25 CP are given in Table 1. We have $A_{\rm AV} = -0.02 \pm 0.48$ and $E_{\rm AV} - 0.60 \pm 0.44$, respectively. For comparison, the asymmetry and excess of the 10.7 year solar cycle (Fig. 3, left panels) are 0.29 and -0.50. The asymmetry and excess of the 1 year planetarium cycle (Fig. 3, right panels) are 0.04 and -0.64, again similar to our CPs.

In Fig. 6(c) the behavior of the excess E, synchronous with the extremely absolute asymmetries A, gives evidences that in cases of $|A| > 0$ the CPs contain frequently high non-central peaks.

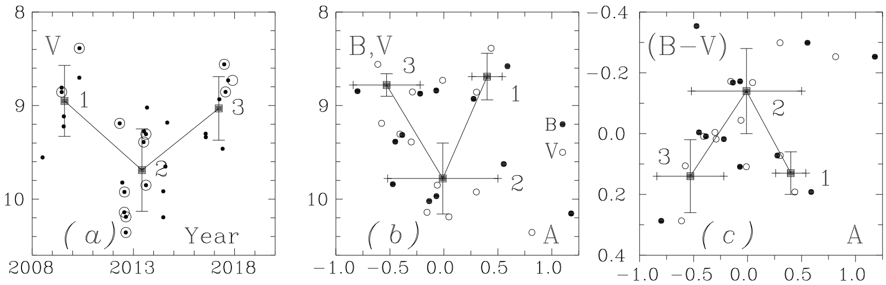

Fig. 7. (a) Brightness evolution of the FS in 2009–2018 (squares) and positions of our selected 13 V LCs (circles) among all 29 V LCs of the FS in the years (dots); (b,c): Juxtaposition of the asymmetry and the average magnitude or color index.

4. Asymmetry of the combined profile versus the brightness and color index of the flickering source

The unveiled tendency of the asymmetry to decrease over the years of observations points out possible dependency between the asymmetry of the CP and the brightness of the FS.

Figure 7(a) shows the average magnitudes of the selected 13 V Lcs among the V magnitudes of the FS in the years. The photometric data are taken from Paper II. Obviously, 5 of 13 LCs belong to the most high bright states of the FS. From the other 8 LCs, 5 correspond to the most faint states of the FS. Analogous segregation by color index is not unveiled. Figures 7(b) and 7(c) represent the correspondences between the CP asymmetry and the FS brightness or color index.

So, in spite of the relatively small variation of the average brightness and color of the FS in the years, the CP asymmetry follows them. Or may be challenges them?

Conclusions

In this paper we derive and analyze 25 combined profiles of time structures in the flickering of RS Oph with quasi-periods 16–35 min, repeating 3–7 times.

We derive that the average SNR of the combined profiles is 28, from 10 to 43 or 14 dB, from 10 to 16 dB (see Table 2). The SNR decreases slightly in the years 2009–2018.

We find that the asymmetry (skewness) of the combined profiles changes over the years form positive to negative, being in average about 0 in 2013–2014. The excess (kurtosis) has average value –0.6.

We found that the higher brightness and redder color index of the flickering source are associated with positive or negative asymmetry of the combined profile.

Usually the flickering phenomenon is explained qualitatively by variable mass transfer from mass donor through the accretion disk to the surface of white dwarf. Then the reasons of the time evolution of the heights and asymmetry of the combined profiles, synchronous with the change of the brightness and color index, are not clear.

Acknowledgments: This work is supported by the grant К*П*-06-H28/2 08.12.2018 (Bulgarian National Science Fund).

The authors are grateful to the anonymous referee for his attention to this paper and for the recommendations.

References

Johnson, Don H., 2006, Scholarpedia, 1(12):2088.
Georgiev, T., Zamanov, R., Boeva, S., et al. 2019, Bulg. Astron. J. 30, 83-98. Paper I
Georgiev, T., Zamanov, R., Boeva, S., et al. 2020, Bulg. Astron. J. 32, p. 35, Paper II
Georgiev, T., Zamanov, R., Boeva, S., et al. 2020, Bulg. Astron. J. 33, p. 3, Paper III
Kundra, E., & Hric, L. 2014, Contributions of the Astronomical Observatory Skalnate Pleso, 43, 459
Kundra, E., Hric, L., & Gális, R. 2010, Binaries - Key to Comprehension of the Universe, 435, 341
Lafler, J., & Kinman, T.D., 1965, ApJS 11, 216
Mikołajewska, J., & Shara, M. M. 2017, ApJ, 847, 99
Shenavrin, V. I., Taranova, O. G., & Nadzhip, A. E. 2011, Astronomy Reports, 55, 31
Walker, A. R. 1977, MNRAS, 179, 587
Wynn, G. 2008, RS Ophiuchi (2006) and the Recurrent Nova Phenomenon, ASP Conf. 401, 73
Zamanov, R. K., Boeva, S., Latev, G. Y., et al. 2018, MNRAS, 480, 1363

Appendix. Combined profiles I. See Sect. 1 and Fig. 2.

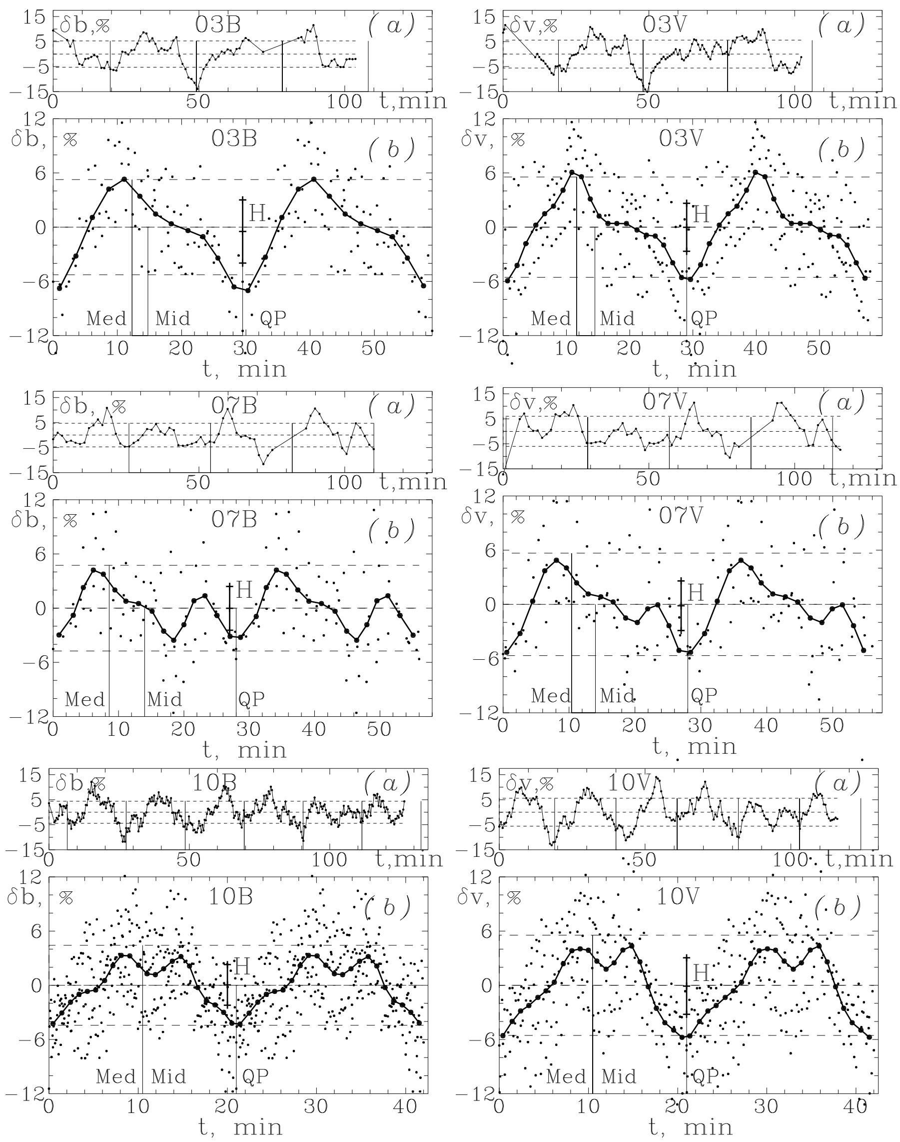

Appendix. Combined profiles II. See Sect. 1 and Fig. 2.

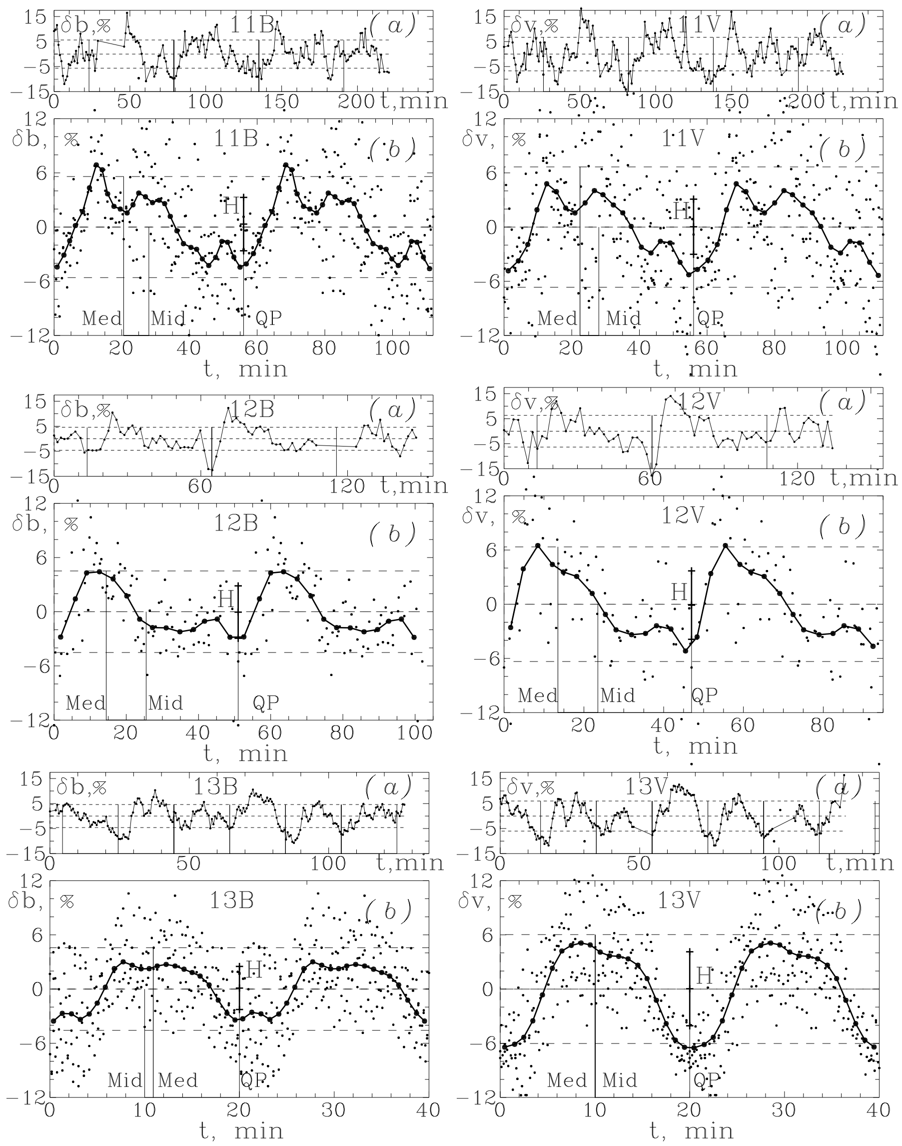

Appendix. Combined profiles III. See Sect. 1 and Fig. 2.

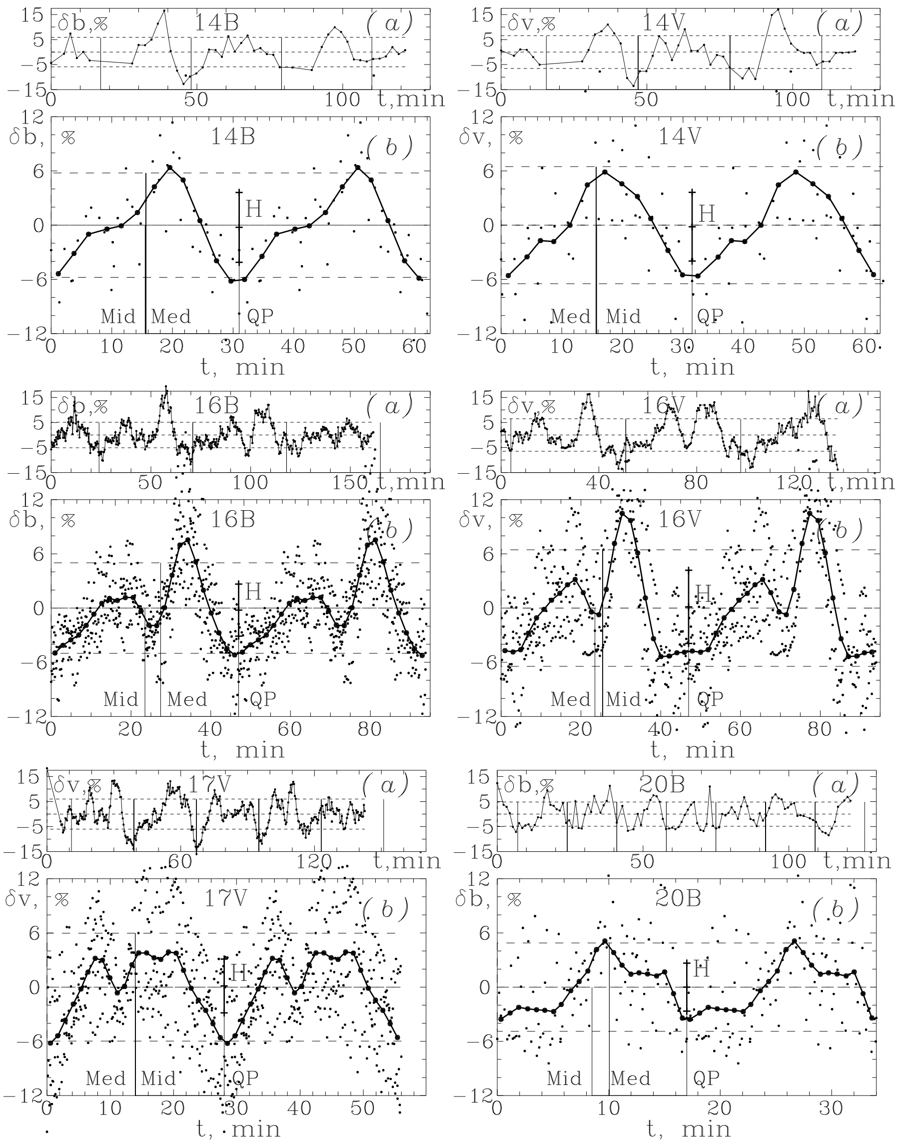

Appendix. Combined profiles IV. See Sect. 1 and Fig. 2.